A STUDY OF THREE-DIMENSIONAL NONLINEAR NIP MECHANICS

by

Ted Diehl[1,2], Kenneth D. Stack[2], and Richard C. Benson[2]

[1]Eastman Kodak Company
Rochester, New York

[2]University of Rochester
Rochester, New York

Abstract

An understanding of nip pressure and deformed nip geometry is of vital importance to the design of web handling equipment. Axial variations in nip pressure and deformed nip geometry can lead to poor product performance and customer dissatisfaction. This study evaluates these axial variations for two general cases: an identical-hollow-drum design and a classic calendering design. Both cases include the effects of elastomeric coverings. Comparisons between modelling the resulting axial variations in nip parameters by beam effects or shell effects are evaluated. Evaluations of nip pressure and overdrive/underdrive are performed. Approximate boundary conditions for the study of web wrinkling are proposed based on deformed nip geometry.

1.0 INTRODUCTION

Figure 1 depicts two common nip designs: two identical hollow drums and the classic calendering geometry. The identical-hollow-drum design consists of two hollow drums of the same geometry, both covered with a thin elastomer. The drums are forced together to form a nip that is capable of transporting and processing a web. Axial variations in nip parameters such as contact pressure and contact area are generated by deformation of the drums and the elastomeric covering. Figure 1c shows an example of the nonuniform contact profile. In the classic calendering design, one rigid roller covered with a thick elastomer is indented by another rigid roller of a potentially different radius. In this case, only the thick elastomeric covering is considered to be deformable. Both of these designs are found in many web handling

situations, including paper making, film manufacturing, paper processing, and office imaging. Axial variations in contact pressure and nip deformation can cause web wrinkling, uneven material transfer, poor image quality, and localized web/elastomer wear.

K. L. Johnson's [1] book on contact mechanics provides an excellent overview of linear elastic, small strain theories applied to nip mechanics. A majority of the work in nip mechanics has focused on plane strain solutions where axial variation in the nip is neglected. Many of these solutions also assume Hertzian contact models. Parish [2,3] has approximated axial variation by including beam-bending effects down the axis of the nip. Keene [4] used a shell on a Winkler foundation to study nonuniform pressure distributions.

Unfortunately, many web handling devices do not exhibit linear-elastic material behavior and often involve nonlinear deformations. Rubber-covered rollers used in calendering operations are a common example. Batra [5] studied the plane strain frictionless indentation of a thick rubber covered roller by a rigid cylinder. Because the deformation was large and the material was not linear elastic, Batra employed nonlinear finite element methods. He compared his solution to the experimental work of Spengos [6] and found good agreement. Stack and Benson [7] have analyzed the axial variations of a rubber covered rigid cylinder indented by a flat, frictionless surface. They found significant axial pressure variations due solely to the rubber deformation.

In this study, it is assumed that the web is extremely thin and flexible and will not affect the nip pressure or nip deformation. The only deformations that will be considered are those of the elastomeric coverings and the hollow drums. Nip parameters of axial pressure uniformity and the axial variation of roller underdrive or overdrive are of primary interest. Figure 2 shows the undeformed and deformed states of a generic, flexible, plane strain roller. As the roller rotates, the deformation causes a speed difference in the outer fiber of the roller between the deformed and undeformed geometries. Because the deformed roller travels at a different speed than that of the undeformed roller, any web driven by the nip travels at a speed not equal to that of the undeformed roller. This speed difference between the web and the undeformed roller is commonly denoted as overdrive or underdrive, depending upon whether the speed ratio is greater or less than unity, respectively.

To obtain the axial variations of nip parameters, we require the use of 3-D solutions. Because of the computational requirements of these solutions, it is desirable to ignore frictional effects due to their increased computational costs. For many cases, the friction forces in the nip are small in comparison to the normal forces. We will assume that friction will not significantly change the nature of the deformed geometry. This allows us to model the rolling friction problem as a frictionless, quasi-static indentation. The solutions we will present will assume that the nip deformation is

symmetric about the center of the nip. The inclusion of frictional effects would add asymmetry to the deformation. It is recognized that frictional effects are important to a complete solution of this problem. However, for this initial investigation, these frictional effects are ignored.

Calculations of contact pressure, nip width, and overdrive/underdrive will be made for a variety of nip geometries. Solutions to nips formed by short, hollow drums will be calculated. Solutions that model the drums as beams or thick shells will be compared to show that beam-bending approximations do not adequately predict the axial variations in nip parameters. The radius ratio of the two rollers in a calendering design will be shown to affect the axial variation of overdrive/underdrive behavior. Approximate boundary conditions for the study of web wrinkling will be proposed based on deformed nip geometry.

2.0 EVALUATION OF SPEED RATIO

As stated in the introduction, an important nip parameter in determining web transport is the axial variation of underdrive or overdrive. Based on definitions from Cole and Piarulli [8], these quantities will be developed using the definition of speed ratio. For ease of development, we consider the case of a generic, flexible, plane strain roller (see Figure 2). Consider a particle denoted as $B(\boldsymbol{X}, t)$ in its undeformed state and $B(\boldsymbol{x}, t)$ in its deformed state. The bold quantities $\boldsymbol{X}$ and $\boldsymbol{x}$ are the position vectors of B in the undeformed and deformed states, respectively.[1] As shown in Figure 2, the particle is located on the outer fiber of the elastomeric covering. During the time increment $\Delta t_{ji} = t_j - t_i$, particle B travels a distance ΔS_{ji} in its undeformed state and Δs_{ji} in the deformed state. In the general nip solution, the distance measurements ΔS_{ji} and Δs_{ji} are measured in a curvilinear coordinate system. The average speed of this particle in both states is then defined as

$$V_{ji} \equiv \frac{\Delta S_{ji}}{\Delta t_{ji}}$$
$$v_{ji} \equiv \frac{\Delta s_{ji}}{\Delta t_{ji}} \tag{1}$$

From these two average velocities, the average speed ratio is defined as

$$\gamma_{ji} \equiv \frac{\Delta s_{ji}}{\Delta S_{ji}} \tag{2}$$

1. In Figure 2, the subscripts i and j applied to the position vectors $\boldsymbol{X}$ and $\boldsymbol{x}$ denote that these vectors will be different at times t_i and t_j.

Taking the limit as Δt_{ji} approaches zero yields the instantaneous speed ratio, λ, defined as

$$\lambda \equiv \frac{ds}{dS} \tag{3}$$

In the finite element model, the quantities ds and dS are approximated as individual finite element lengths. The instantaneous speed ratio, λ, is also equal to the local stretch ratio in the curvilinear coordinate system of a material particle located on the outer fiber of the nip. Integrating the instantaneous speed ratio, $\lambda(t)$, over the time increment Δt_{ji} yields the average speed ratio, γ_{ji}

$$\gamma_{ji} = \frac{1}{\Delta S_{ji}} \int_{t_i}^{t_j} \lambda(\tau)\, d\tau \tag{4}$$

By these definitions, we obtain relative velocity information from a static solution. This method represents an Eulerian viewpoint of a Lagrangian solution.

The bounds of the nip are defined by the locations where the contact pressure becomes zero and are denoted as $S = \pm A$ and $s = \pm a$ in the undeformed and deformed states, respectively. Figure 2c shows a typical symmetric nip pressure profile. For the conditions depicted in Figure 2a and Figure 2b, the times t_i and t_j are arbitrarily chosen at the beginning and end of the nip. If these times are symmetrically chosen closer to or farther from the center of the nip, different values of the average speed ratio are computed. This is shown in Figure 2d. Note that $\gamma - 1$ has been plotted since γ typically has values close to unity. For overdrive, $\gamma - 1 > 0$, and for underdrive, $\gamma - 1 < 0$. Note that far from the nip, $\gamma - 1 \rightarrow 0$ as the roller deformation approaches zero. Figure 2e depicts a similar plot for the instantaneous speed ratio, λ. Again, $\lambda - 1$ is plotted. For a symmetric nip, we have

$$\gamma(s=0) = \lambda(s=0) \tag{5}$$

We have only defined the deformation and overdrive/underdrive of the elastomeric nip. Of course, we would like to relate these quantities to the subsequent behavior of the web. We have assumed that decoupling the web deformation from that of the nip is valid. In actuality, the web/elastomer system is coupled because the system will exhibit regions of stick and slip. The fully coupled solution for a 3-D problem is extremely expensive. Assuming that the frictional effects from the web would not significantly affect the nip deformation, we can assume that, inside the nip, the maximum and minimum values of either the average speed ratio or instantaneous speed ratio of the elastomer will bound[1] the values of underdrive/overdrive for the web.

---

1. Although these bounds are not exact due to frictional and web deformation affects that have been ignored, they provide an approximate estimate of these bounds.

One common cause of web wrinkling is axial variations in transport conditions. In predicting web wrinkling, the axial variation of γ is more important than the actual value of γ itself. Different nip configurations will lead to different forms of axial variation. The subsequent web behavior will be a function of these variations.

3.0 PLANE STRAIN SOLUTIONS

Before discussing full 3-D solutions, several plane strain cases are evaluated to determine proper mesh sizes, solution technique (need for large-strain calculations), and material law (Hooke's law or hyperelasticity). Proper mesh density is essential for efficient computations. Theoretically, for a symmetric plane strain model, 180 degrees must be modeled. However, for the nip solutions presented in this study, the deformation is localized near the nip region and only a partial model[1] is required. As seen in Figure 3, all meshes are biased to have smaller elements near the edge of the nip. This provided a more accurate measure of nip width and other nip parameters.

All solutions of nip deformation and contact pressure were computed using the nonlinear finite element code ABAQUS/Standard V5.2 [9]. This code includes algorithms for large strain, nonlinear material laws, and general contact between flexible and rigid bodies. Calculations of average speed ratio and instantaneous speed ratio were postcalculated based on displacements from the finite element solutions.

The general method that is used to model the elastomeric coverings is a hyperelastic strain energy density function. A one-term Ogden-Hill formulation [9] was used to model the rubber-like elastomers. This law is defined as

$$U = \frac{2\mu}{\alpha^2}\left(\bar{\lambda}_1^{\alpha} + \bar{\lambda}_2^{\alpha} + \bar{\lambda}_3^{\alpha} - 3\right) + \frac{1}{D}(J-1)^2 \tag{6}$$

where $\bar{\lambda}$ equals $J^{-1/3}$ times the principal stretch ratio and J is the Jacobian of the deformation tensor. The parameters, μ, α, and D are material parameters. For a neo-Hookean material, μ equals the initial tangent shear modulus, D equals two divided by the initial tangent bulk modulus, and α equals two. For small strains, this form reduces to Hooke's law. Hence, if the nip deformation is small (i.e., a stiff nip), Hooke's law is sufficient (provided $\nu \neq 0.5$). For nips with larger deformations, the Ogden-Hill formulation will be necessary to correctly model the nonlinear material behavior.

For this study, two types of elastomers were investigated: a "hard" elastomer and a "soft" elastomer. The hard elastomer had an initial Young's modulus of 172 MPa and an initial Poisson's ratio of 0.45. The soft elastomer had an initial Young's modulus of 1.72 MPa and an initial Poisson's ratio of 0.45.

1. For the geometries in this study, the models ranged from 10 to 60 degrees in the hoop direction.

For the plane strain solutions, only the elastomeric coverings were considered. The geometry is depicted in Figure 3. Figure 4 presents the solutions of nip pressure, average speed ratios, and instantaneous speed ratios for both hard and soft elastomers. Both linear (Hooke's law and small strain) and nonlinear (Ogden-Hill law and large strain) solutions are computed.[1] In all cases, an applied load of 8.76 kN/m was applied.[2] For the hard elastomer simulations, both linear and nonlinear solutions produced very similar solutions. For the soft elastomer, the results between linear and nonlinear solutions differ substantially. Although the pressure results are similar, the speed ratio results are quite different with a maximum variation of 30% between linear and nonlinear solutions. Based on these solutions, all 3-D simulations that contain the hard elastomer will use the linear solution technique while all 3-D simulations that contain the soft elastomer will use the nonlinear solution technique.

4.0 THREE-DIMENSIONAL EFFECTS

For all of the cases in this section, the axial length of the rollers (not including the shafts) was 28 cm. Due to symmetry arguments, only half of the axial length was modelled. Due to other symmetry arguments previously stated, symmetry conditions were also applied about the center ($s = 0$) of the model. The following solutions compare the nip behavior and axial variations due to the drum deflections and the free edge effect of the elastomeric coating.

4.1 Identical-Short-Hollow-Drum Design

Figure 5 shows both the shell and beam models used to analyze this design. The models take full advantage of all symmetry previously discussed. The drum is made of aluminum with an internal radius of 7.6 cm and an external radius of 8.4 cm. The end-cap of the drum has a thickness of 0.8 cm. The drum has a solid aluminum shaft attached to the end-cap that is 8.0 cm long, 3.5 cm in radius, and is simply supported. The shell model uses elements that include transverse shear flexibility. The equivalent beam model assumes Timoshenko beam theory with shear flexibility. Inclusion of shear flexibility in the beam model reduces the nominal bending stiffness predicted by only Euler-Bernoulli bending by approximately 40%. The drum in the beam model is connected to the elastomer by rigid MPC's (multipoint constraints). For all models, the thickness of the elastomer is 0.2 cm. For all analyses of this design, the nominal applied loading was 8.76 kN/m. Since the total drum length (not including the shafts) is 28 cm, this is equivalent to a total load, F, equal to 2.45 kN (see Figure 1a).

Figure 6a shows the deformed shape of the drum (magnified 1000 times) in the shell model for a simulation with the hard elastomer. As seen in the figure, the drum

1. Both solutions include a nonlinear contact algorithm.

2. The load of 8.76 kN/m is equal to a load of 8.76 kN per every meter of depth in the plane strain model.

"indents" more at the middle of the drum (z = 0 cm) than near the end-cap. This is due to the increased hoop stiffness that the end-cap provides for the drum. A similar deformed shape results with the soft elastomer. Figure 6b shows the drum deflections relative to the end-cap deflection. For the beam models, the deflection is taken about the centroid of the beam since it is rigidly attached to the elastomer with MPCs. As seen in the plot, the shell models predict greater relative deflection than the beam models. It is interesting to note that for the shell models, the design with a hard elastomer produced less relative drum deflection than the design for the soft elastomer. This result appears counterintuitive but is explained as follows. With a hard elastomer, the contact pressure is concentrated more near the end-caps than for the soft elastomer which more evenly distributes the load over the entire length of the drum (see Figure 7 and Figure 8). By careful inspection of Figure 6b, it is seen that near the end-cap (z = 14 cm), the relative shell deflection is larger for the hard elastomer model than for the soft elastomer model.

These axial variations in drum deflections are the primary cause of axial variations in nip parameters for this design. As such, we see that the shell solution predicts a much greater axial variation as well as greater sensitivity to the stiffness of the elastomer. If the cylinder is long, slender, and thick, then beam approximations to the shell behavior are valid. However, for short, thin-walled cylinders, shell effects must be included.

Figure 7 and Figure 8 show how the contact pressure, nip width, average speed ratio, and instantaneous speed ratio vary both across the nip and down the nip (axially). The highest pressure is nearest the end-caps. Note that this peak pressure is not exactly at the end of the drum, but slightly inside the drum (z < 14 cm). This is due to the free-edge effect of the elastomer. At the end of the drum, the elastomer is not constrained and will tend to behave softer. The variations in average speed ratio and instantaneous speed ratio follow similar trends. In all the plots, the speed ratio is greatest nearest the peak pressure point. The noise in the average speed ratio calculations and especially the instantaneous speed ratios in due to the coarseness of the mesh used for solutions. A more refined mesh would produce smoother results. As seen by all the plots in Figures 6-8, the shell solution predicts much greater axial variation than the beam model.

4.2 Classic Calendering Design

Figure 1b shows the geometry of a classic calendering design. The problem was initially modelled using a symmetry length of 14 cm. After examining the solutions, it was determined that the plane strain region of the deformation was fairly large (approximately 5.1 cm). The model was shortened to 7.9 cm (Z = 5.1 cm to Z = 14.0 cm) in order to analyze the non-plane-strain behavior in more detail. These shortened results still match the plane strain boundary condition in the middle of the axis and are therefore accurate. For these models, an imposed displacement of 0.55 cm

was used. The elastomeric material had an initial Young's modulus of 1.72 MPa and an initial Poisson's ratio of 0.45. Because the deformation was large, the nonlinear solution technique was employed.

Changes in the noncovered rigid-roller size were found to affect the behavior of the nip. Figure 9 compares contact pressure, average speed ratio and instantaneous speed ratio for two different rigid rollers which had radii of 2 cm and 6 cm, respectively. Figure 9d shows the pressure profile in the nip for a rigid-roller radius of 6 cm. As expected, the pressure is highest at the center of the nip (z = 0 cm) and drops off towards the edge (z = 14 cm). This is due to the free-edge effects as discussed previously. For both cases in Figure 9, the average speed ratios are greater than unity, meaning that in an average sense, the nip is experiencing overdrive everywhere. But, for the instantaneous speed ratios, the rigid-roller radius of 6 cm produces both overdrive and underdrive within the nip. The rigid-roller radius of 2 cm produces only overdrive. In comparing the two cases, we can see that, while the pressure profiles are similar, the amount of overdrive and underdrive is increased for a rigid-roller radius of 2 cm. This change is due purely to geometry. Notice also that the variation in overdrive down the axis of the nip (s=0) is also increased by decreasing the rigid-roller radius. It is this variation that can lead to wrinkling in thin webs.

4.3 Approximate Boundary Conditions For Web Wrinkling Analysis

Having calculated the axial variations of the nip parameters, we now present an approximate method of determining the "form" of the boundary conditions that would likely exist on the web. As stated previously, we have decoupled the web from the nip solution and ignored the actual stick/slip behavior that occurs in the nip. Because of these assumptions, only the general form of the boundary conditions can be predicted. Based on the speed ratio equations (equations 1-3), we can obtain the form of the variation of displacements in the web transport direction. These variations are the boundary conditions that would be applied in a web wrinkling analysis. The boundary conditions can be computed based on either the average speed ratio or the instantaneous speed ratio formulations. Cole and Piarulli [8] used the average speed ratio computed over the entire nip width in plane strain analyses to compare against experiments. They found acceptable agreement. For brevity, we will define the approximate web boundary conditions based on the average speed ratio, γ. The instantaneous speed ratio can also be used by substituting λ for γ in the following discussion.

For a drum with a uniform outer radius in the undeformed configuration, the normalized displacement boundary condition is defined as

$$\delta(z, s) \equiv \frac{\gamma(z, s)}{\gamma(z=0, s)} \tag{7}$$

where $\delta(z,s)$ is the normalized displacement boundary condition.[1] The boundary condition is normalized relative to the axial middle of the drum ($z = 0$). The actual normalized boundary condition that is applied in a wrinkling analysis is $\delta(z,s=b)$ where b is bounded by the center of the nip (b=0) and the edge of the nip (b=a). Figure 10 shows some sample calculations for the 3-D models previous computed. Note that the value of $100\cdot(\delta(z,s) - 1)$ is plotted since typical values of $\delta(z,s)$ are near unity.

Figure 10a depicts approximate web boundary conditions for the identical hollow drum design with a hard elastomer. Both beam and shell solutions are presented. The shell solution shows greater variation in the boundary condition. For each model type (beam or shell), the normalized boundary conditions have been computed at the bounds: the center of nip ($s = 0$ cm) and near the edge of the nip ($s \approx a$). For the hollow-drum design, the web will travel faster near the edge of the drum ($z \approx 13$ cm) than in the middle ($z = 0$ cm). At the far edge of the drum ($z = 14$ cm), the free-edge effect is pronounced and causes the web to decrease in speed relative to the maximum speed value (at $z \approx 13$ cm). The oscillatory nature of the answers in Figure 10 are again due to the coarseness of the mesh and would improve with a finer mesh.

Figure 10b depicts the approximate web boundary conditions for the classic calendering problem. As the radius of the rigid roller decreased, both the amount of overdrive and the axial variation of overdrive increased. Like the solutions to the identical-hollow-drum problem, at the free edge the web speed decreases. Again, a finer mesh would be needed to improve the oscillatory nature of the solution, but we believe that this solution does predict the correct general behavior. See Stack and Benson [7] for a similar solution using a more detailed mesh.

Comparing Figure 10a and Figure 10b we see that the resulting approximate web boundary conditions generated by the two designs are quite different. The identical-hollow-drum design yields a normalized displacement boundary condition for the web that has a general concave profile. The classic calendering design yields a profile that is generally convex. This difference in profiles can lead to markedly different web transport behavior. It is possible to arrive at a set of elastomeric material constants, elastomeric thickness, and drum geometry that can minimize the variations. It is noted that both nip designs may still exhibit variations near the free edge.

5.0 CONCLUSIONS

Axial variations in nip pressure and deformed nip geometry have been studied for two nip configurations: an identical-short-hollow-drum design and a classic calendering design. Both the average speed ratio and instantaneous speed ratio were

1. If the drum outer radius is not uniform in the undeformed state, then Equation 7 must be modified to take into account the undeformed axial variations of outer-fiber speed ratio that would exist.

computed to determine overdrive/underdrive conditions in the nip. Axial variations in nip parameters for the identical-hollow-drum design were studied with models that simulated the drum deflection by Timoshenko beam theory and thick-shell theory. The primary cause of axial variations in nip parameters was the axial variation in the drum's deflection. The shell models predicted much greater axial variation than the beam models due to localized shell effects. Near the free edge of the nip, edge effects in the thin elastomeric covering on the drums became dominant. For the classic calendering problem, only the free-edge effect of the thick elastomeric covering caused axial variations in nip parameters. Decreasing the radius of the noncovered rigid roller was found to increase both measures of speed ratio and their axial variations. Approximate boundary conditions for the study of web wrinkling have been proposed based on a normalized displacement variation calculated from the axial variations in either the average speed ratios or the instantaneous speed ratios throughout the nip.

Acknowledgments

The authors gratefully acknowledge the financial support of Eastman Kodak Company. Special thanks to Kevin Cole of Eastman Kodak Company for his insightful technical discussions into the analysis of speed ratios, underdrive, and overdrive.

6.0 REFERENCES

[1] Johnson, K. L., Contact Mechanics, Cambridge University Press, Cambridge, 1989.

[2] G. J. Parish, "Measurements of Pressure Distribution Between Metal and Rubber Covered Rollers," British Journal of Applied Physics, Vol. 9, April 1958, pp 158-161.

[3] G. J. Parish, "Calculation of the Behaviour of Rubber-Covered Pressure Rollers," British Journal of Applied Physics, Vol. 12, July 1961, pp 333-336.

[4] Keene, F., Personal Communication, 1991.

[5] R. C. Batra, "Rubber Covered Rolls-The Nonlinear Elastic Problem," Journal of Applied Mechanics, Vol. 47, March 1980, pp 82-86.

[6] A. C. Spengos, "Experimental Investigation of Rolling Contact," Journal of Applied Mechanics, December 1965, pp 859-865.

[7] Stack, K. D., Benson, R. C., "The Effects of Axial Variation in Nip Mechanics," Proceedings of the Second International Conference on Advanced Mechatronics, Meiji University, Tokyo, Japan, 1993.

[8] Cole, K., Piarulli, V., Personal Communication, 1993.

[9] ABAQUS/Standard User's Manual, V 5.2, 1992.

(a) Identical-hollow-drum problem: two identical hollow drums covered with an elastomer

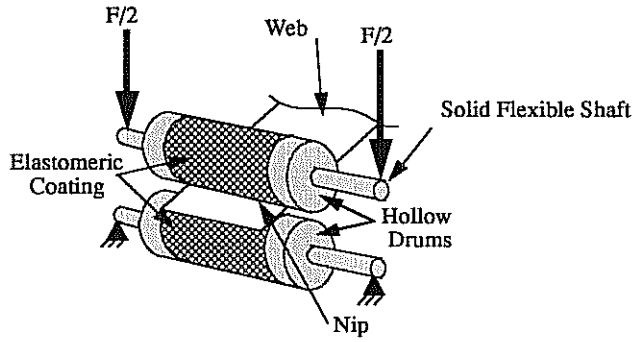

(b) Classic calendering problem: two rigid drums with different diameters, one is covered with an elastomer

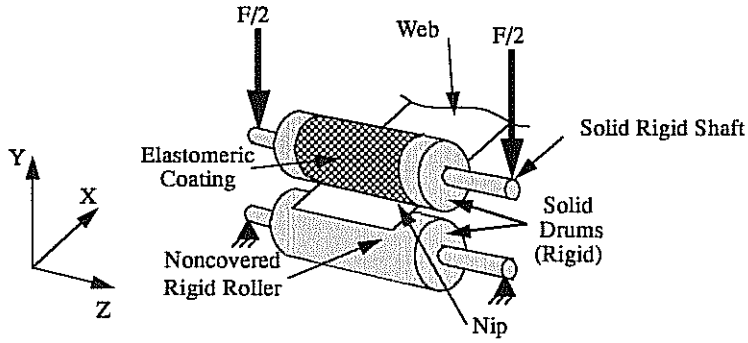

(c) Nonuniform nip contact profile on web

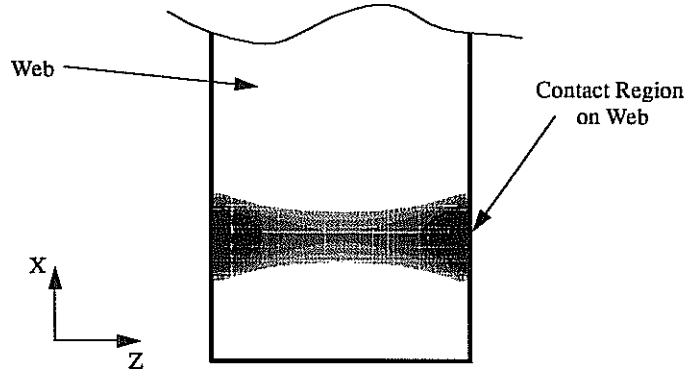

FIGURE 1. Schematic of 3-D nip mechanics problem

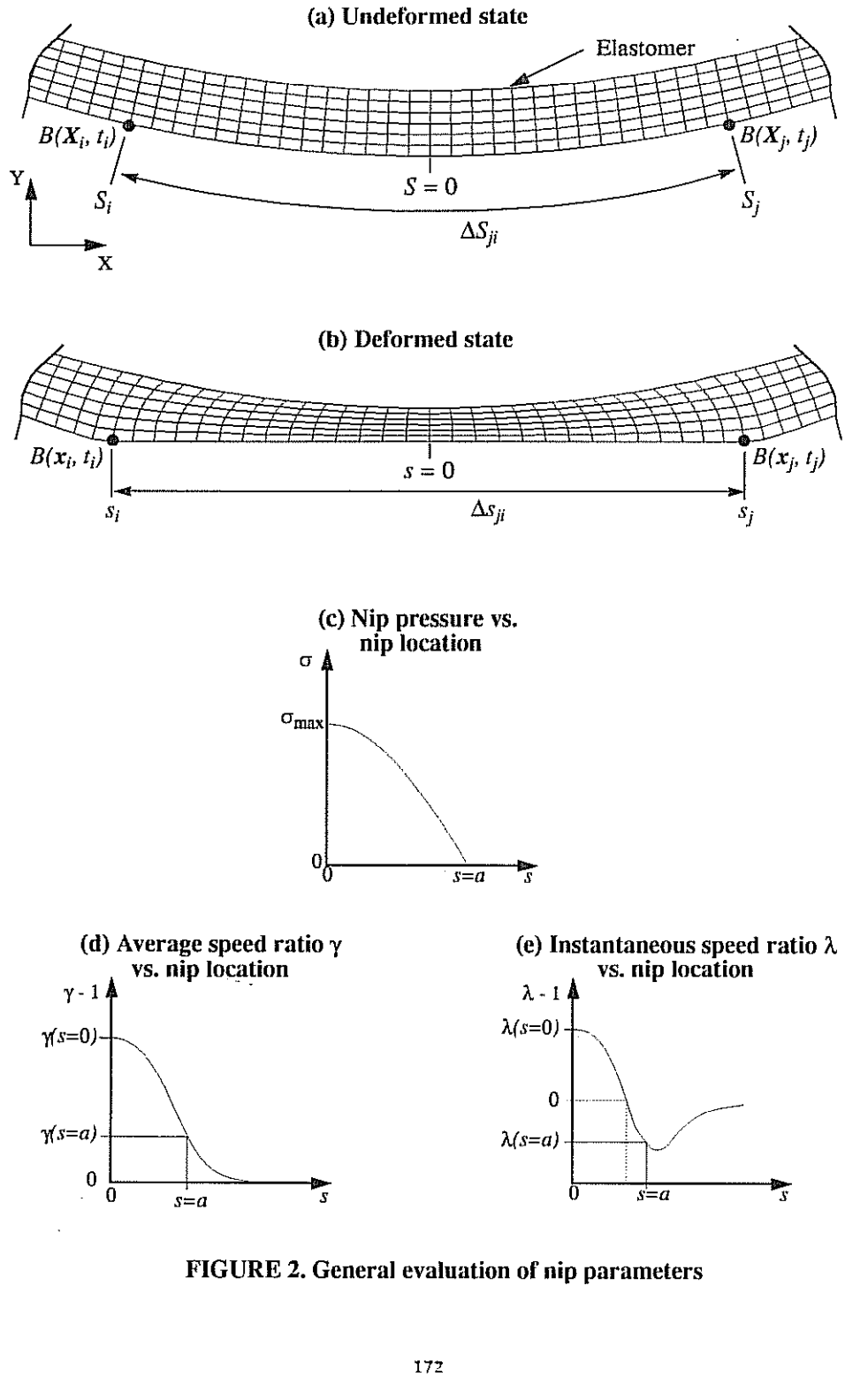

FIGURE 2. General evaluation of nip parameters

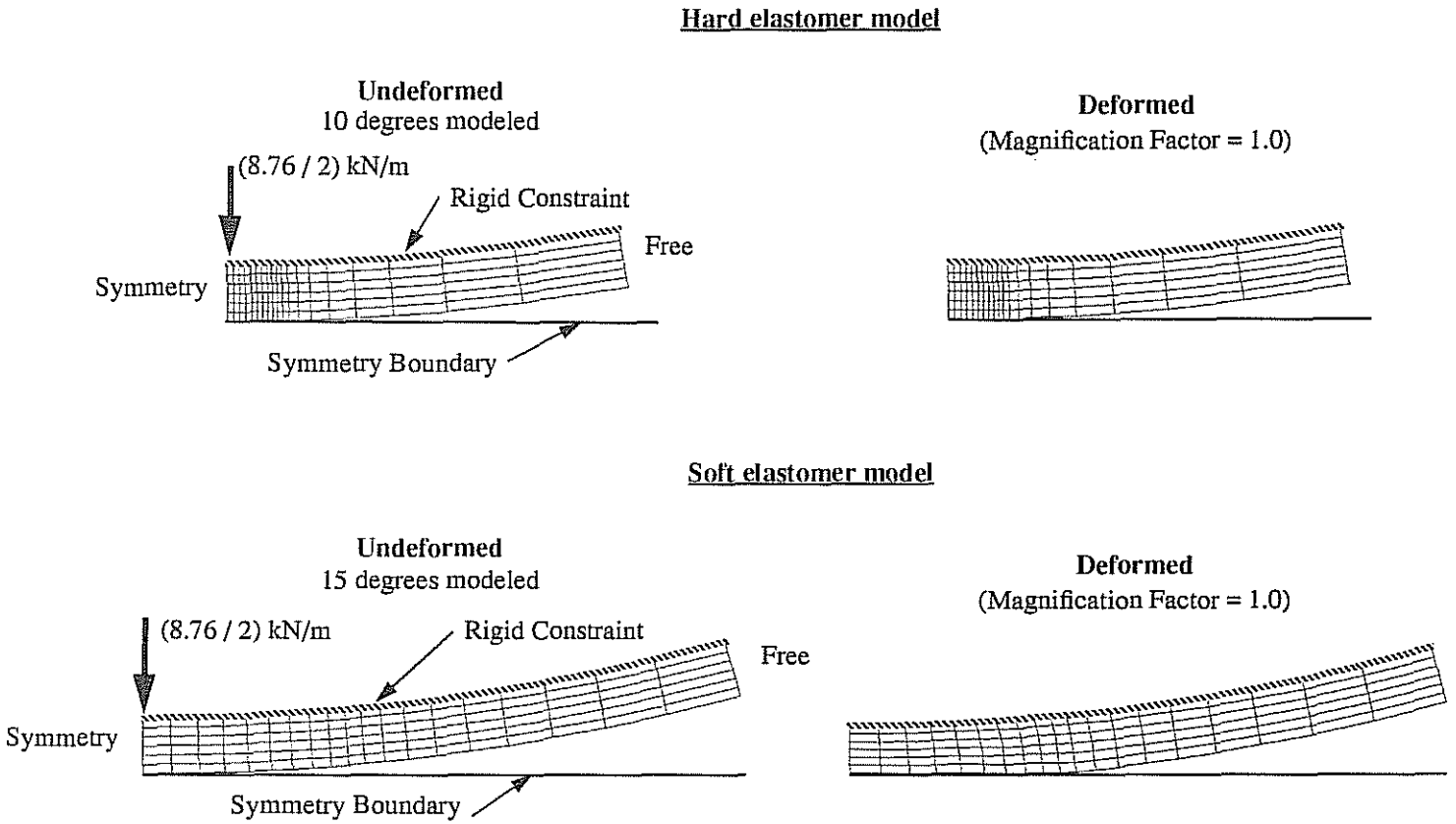

FIGURE 3. Typical meshes used for plane strain solutions: inner radius = 8.0 cm, outer radius = 8.2 cm

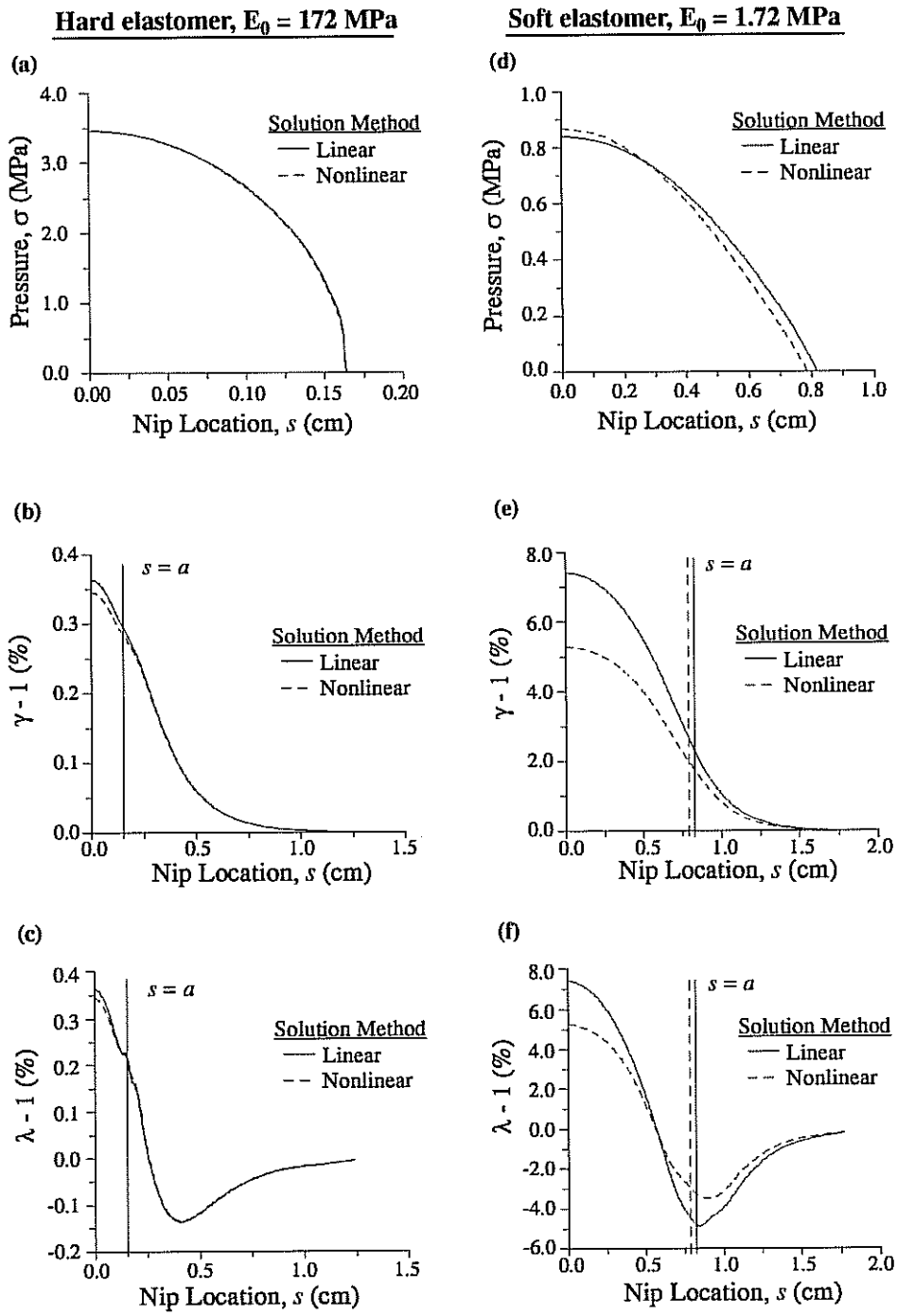

FIGURE 4. Results from plane strain analysis: (a-c) - hard elastomer, (d-f) - soft elastomer. Loading = 8.76 kN/m

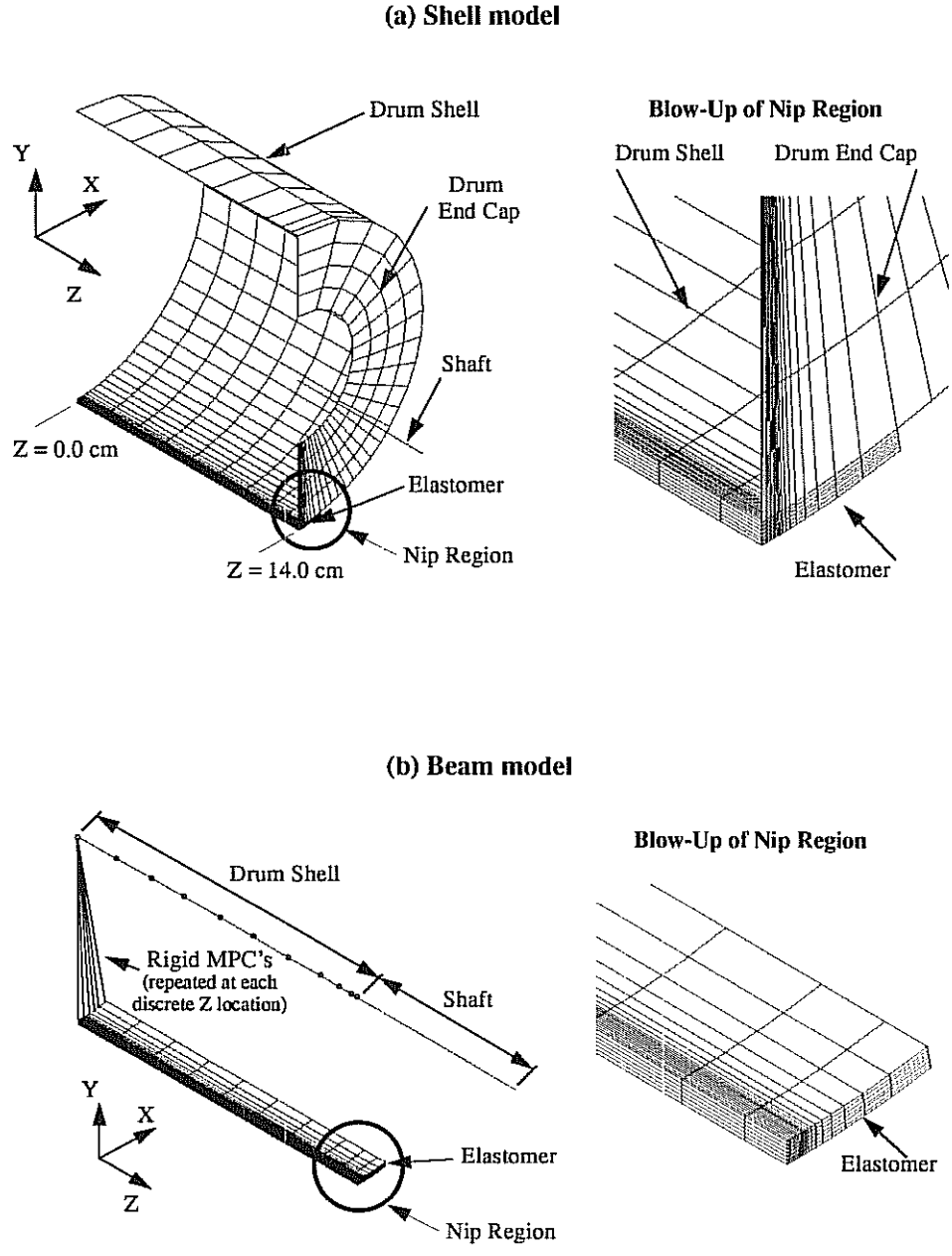

FIGURE 5. Finite element models used to evaluate the identical, short, hollow-drum design.

(a) Deformed drum shape for shell model with hard elastomer (magnification factor = 1000)

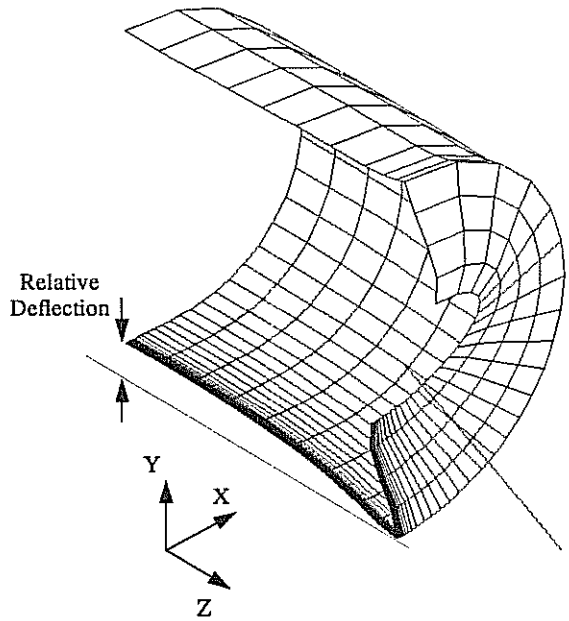

(b) Y-Coordinate deflection of drum relative to edge of drum (various solutions)

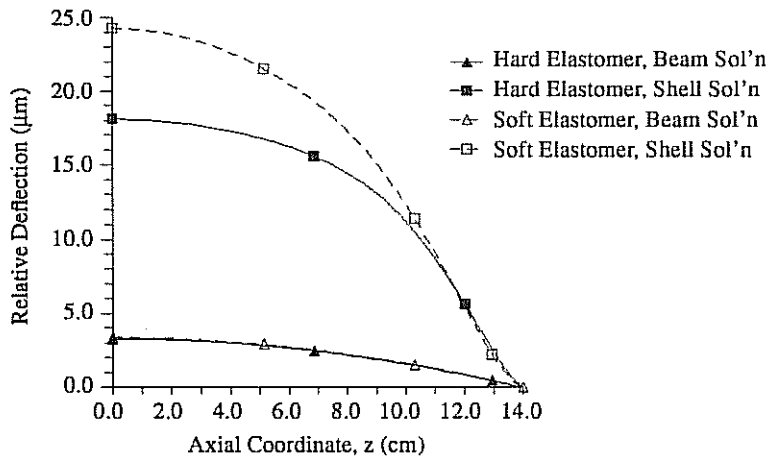

FIGURE 6. Primary cause of axial variation in drum parameters: drum deflections.

Beam model

(a) Normal contact pressure (b) Average speed ratio (c) Instantaneous speed ratio

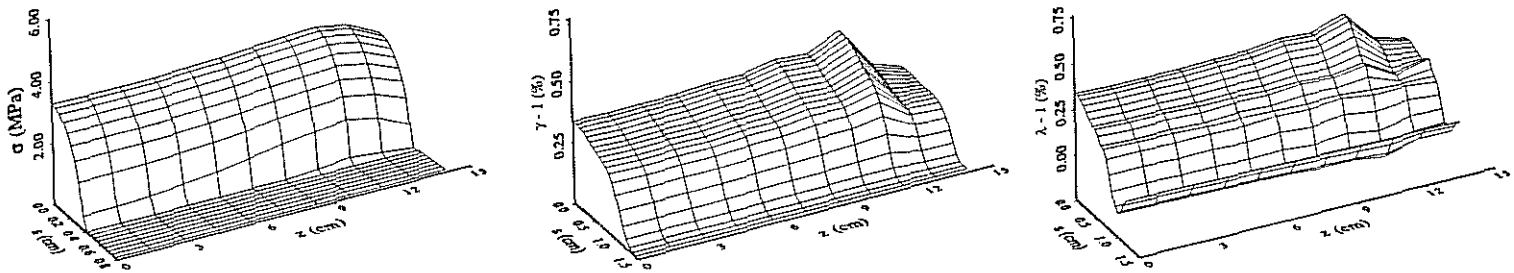

Shell model

(d) Normal contact pressure (e) Average speed ratio (f) Instantaneous speed ratio

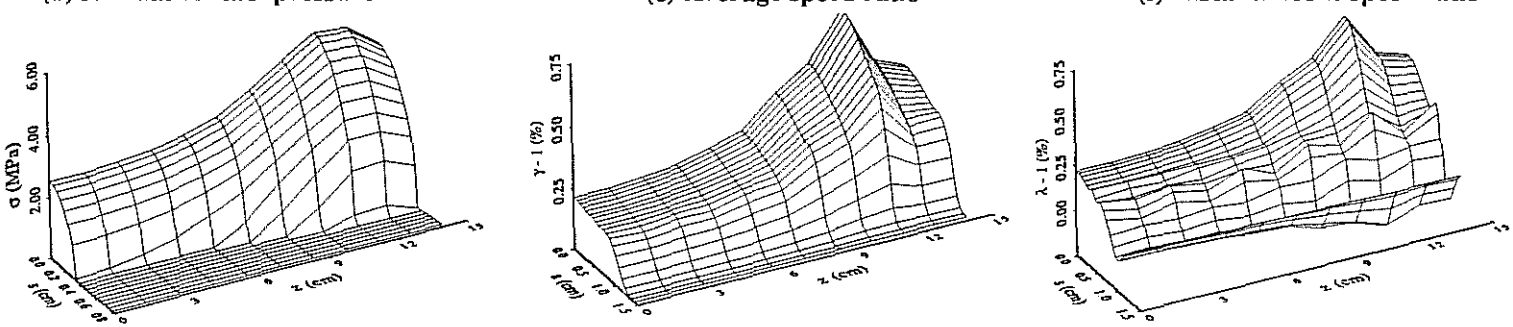

FIGURE 7. Axial variation of pressure, average speed ratio, and instantaneous speed ratio for hollow-drum design: hard elastomer simulations

Beam model

(a) Normal contact pressure

(b) Average speed ratio

(c) Instantaneous speed ratio

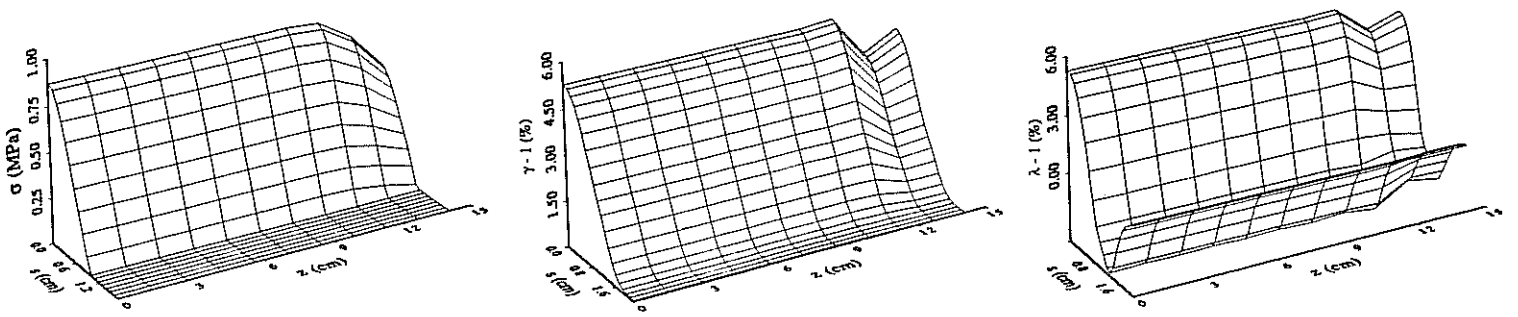

Shell model

(d) Normal contact pressure

(e) Average speed ratio

(f) Instantaneous speed ratio

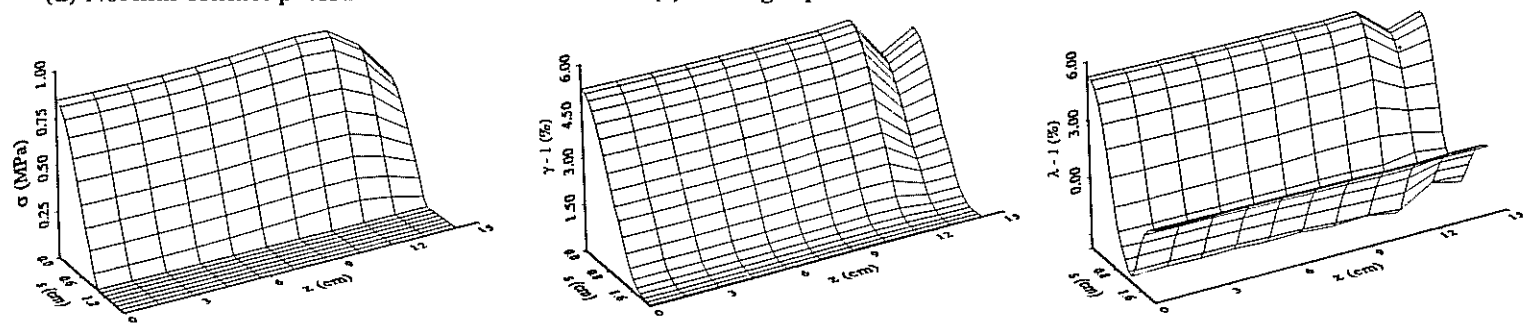

FIGURE 8. Axial variation of pressure, average speed ratio, and instantaneous speed ratio for hollow-drum design: soft elastomer simulations

Noncovered rigid-roller radius = 2 cm

(a) Normal contact pressure

(b) Average speed ratio

(c) Instantaneous speed ratio

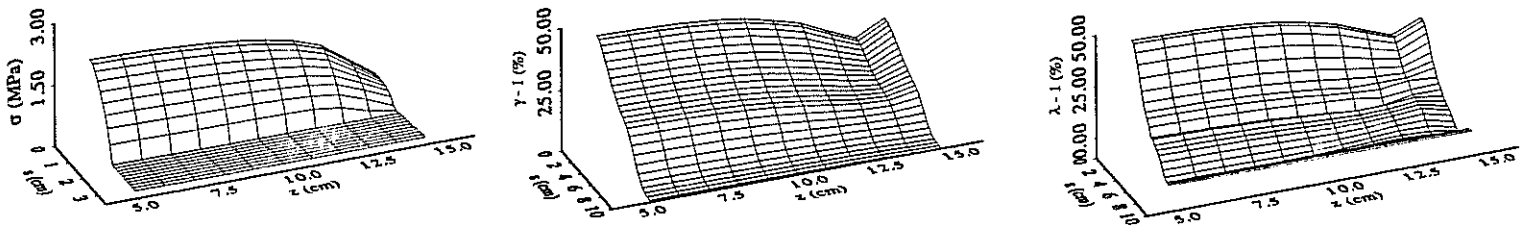

Noncovered rigid-roller radius = 6 cm

(d) Normal contact pressure

(e) Average speed ratio

(f) Instantaneous speed ratio

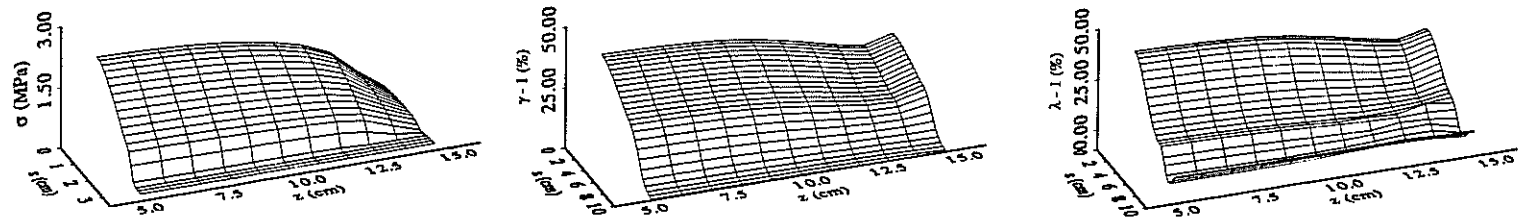

FIGURE 9. Axial variation of pressure, average speed ratio, and instantaneous speed ratio for calendering design: soft elastomer.

(a) Normalized speed ratio for identical-hollow-drum design (hard elastomer)

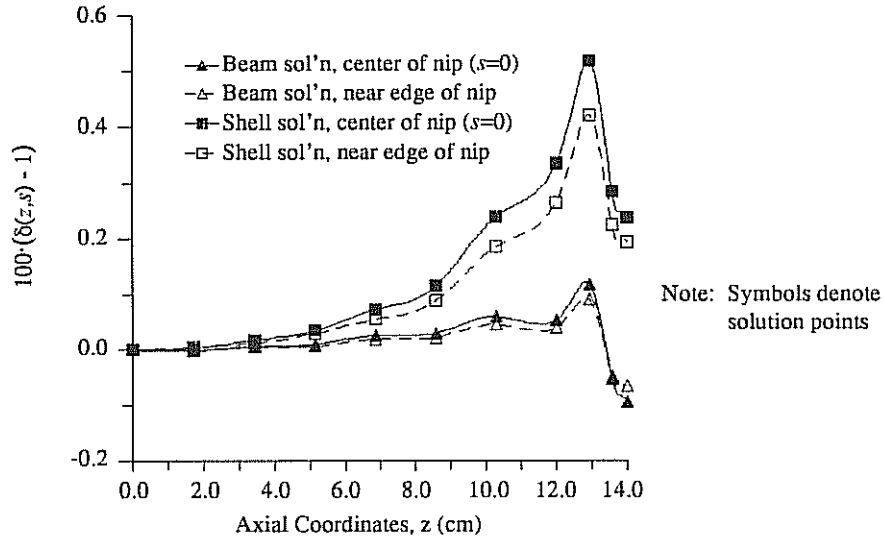

(b) Normalized speed ratio for calendering design

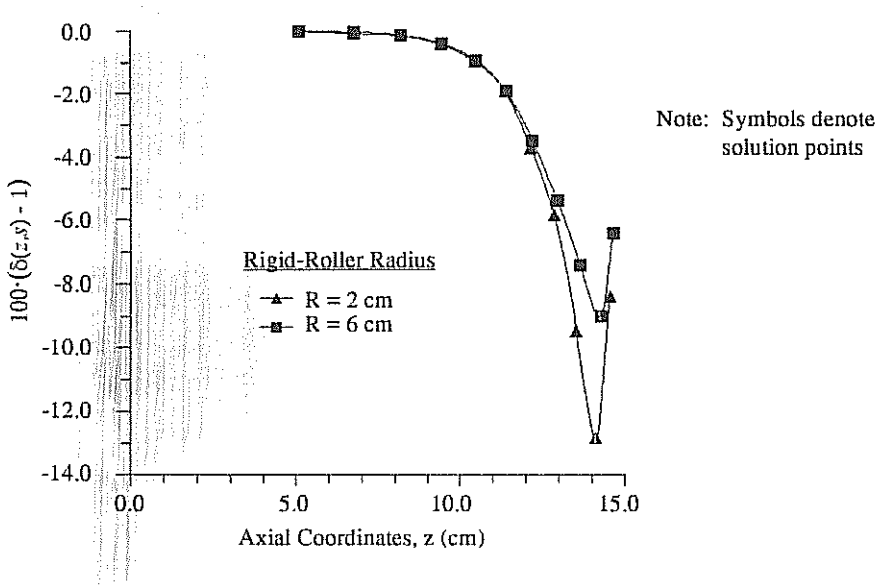

FIGURE 10. Average speed ratio variation normalized to value at middle of drum (z = 0 cm)

QUESTIONS AND ANSWERS

Q. What were the thicknesses of the elastomeric coatings used in the analysis?

A. For the identical-short-hollow-drum design the elastomer was relatively thin: 0.2 cm. For the classic calendering design, the elastomer was relatively thick: 1.3 cm.

Q. How do you handle the Hertzian contact profile?

A. Actually, the solution method goes beyond Hertz contact theory. We are using a nonlinear finite element technique to compute the general contact constraints. The contact algorithm uses Lagrange multipliers to enforce the contact constraint and the whole nonlinear structural problem is solved using Newton-Rapshon iteration. No assumptions of contact pressure profile are assumed with this method.

Q. My question is, in several of your figures you have a beam solution and a shell solution. I was wondering, you led me to believe from your talk that you thought the shell solution was more accurate, and my question is why?

A. The primary problem that I investigated was the identical-short-hollow-drum design. In this design the drum is short, not long and slender like a typical wide-web application. For the case of short hollow drums, local shell-type deformations are dominant. Global beam-type bending is only dominant for long slender roller applications. The shell models allow for additional flexibility that does not exist in the beam models. Furthermore, we have experimental evidence that shell models are required for accurate modeling of problems like the identical-short-hollow-drum design. From a beam-bending viewpoint, axial variations in pressure would be minimized by increasing the bending stiffness of the beam. One method of doing this, without changing the radius of the drum, is to add internal ribs that run axially down the length of the drum. However, from the shell model, we see that the drum needs to have greater hoop stiffness near the center of the drum. Based on this theory, hoop ribs would be added to the drum (these ribs are in an orthogonal direction to the axial rib modification). Models of all three designs were made: no ribs, axial ribs, and hoop ribs. The axial ribs made no significant improvement over the ribless design. The hoop ribs made a dramatic difference in minimizing the axial variation in nip pressure. Experimental measurements on actual castings of these three designs produced the same conclusions.

Q. Your slides show that there is a lot of shear at the elastomer-drum interface but that no shear exists at the nip surface (interface between elastomer and media, modeled as a symmetry boundary). My work indicates that there is a lot of shear at the nip interface.

A. There is no shear at the nip surface because the solutions were computed as frictionless indentations. The main goal of the solutions was to analyze the predominant affect that causes media overdrive: hoop strain in the elastomer. Hence, this analysis is a first step toward the complete solution. We recognize that friction is important and we are currently adding it to the analysis.

However, for 3-D analysis, solutions with friction are very computationally expensive. This analysis only looked at the predominant 3-D affects; axial variation of hoop strain in the elastomer. Including friction into the calculations must be done with great care. Friction is like plasticity, it is path dependent. Thus any solution with friction must be computed as a history developed solution.

Q. You have kind of an unusual condition because you have rolls of identical elastomer present. The rolls are symmetrical. Most of us are using elastomer against hard rolls or similar designs like that.

A. The second problem analyzed in our paper looks at a classic calendering design. That problem has one relatively rigid roller pressing against one elastomer-covered roller. In certain copier-type applications, designs with identical elastomer-covered drums are common. The beauty of finite element solutions is that modification of geometry like that is fairly easy to do. Also, various asymmetries can be included, however, the cost of the solution will increase. For this paper, we wanted to demonstrate the theory and equations with some simple designs. To make the computations quick, we exploited as much symmetry as possible.

Q. How long can these computations take?

A. On a Sun SPARCstation 10, the plane strain solutions take about 3 minutes. The 3-D shell solutions, if you do not take advantage of the fact that the shell deformation is linear, require about 40 minutes. If you use superelement techniques for the shell portion and only perform nonlinear iteration on the elastomer and contact, the solutions take about 10 minutes. Now, if you add friction, the solution times increase substantially.

Q. What was the Poisson's ratio of the Elastomer?

A. The elastomer was modeled as nearly incompressible with an effective Poisson's ratio of 0.45. The beauty of hyperelasticity is the one can model a totally incompressible formulation or a totally compressible formulation. To model totally incompressible material with Hooke's law requires several constitutive manipulations that most commercial finite element codes can not perform.

A. (These was no question for this, just an additional comment by the Author) One other point that I would like to make. In the literature and industry, you will find several people say "It's rubber, it's incompressible". Well, that is simply not true. Nothing is incompressible. If a material was, its wave speed would be infinite. The use of incompressibility is a modeling assumption, just like any other. For certain solution methods, making an assumption of incompressibility makes solution to the problem easier.